[redacted] 62-71976 Copy 681
NASA TM X-152

NASA TM X-152

GPO PRICE $ ________

OTS PRICE(S) $ ________

Hard copy (HC) 1.00

Microfiche (MF) .50

X-7-6

# TECHNICAL MEMORANDUM

## X-152

## INVESTIGATION OF A 4.0-INCH-MEAN-DIAMETER FOUR-STAGE REENTRY TURBINE FOR AUXILIARY POWER DRIVES

By Robert Y. Wong, David L. Darmstadt, and Daniel E. Monroe

Lewis Research Center
Cleveland, Ohio

N65-12795 (ACCESSION NUMBER) 24 (PAGES) TMX-152 (NASA CR OR TMX OR AD NUMBER) (THRU) 1 (CODE) 03 (CATEGORY)

FACILITY FORM 602

~~DECLASSIFIED - EFFECTIVE 1-15-64~~
Authority: Memo Geo. Drobka NASA HQ.
Code ATSS-A Dtd. 3-12-64 Subj: Change
in Security Classification Marking

[redacted]

NATIONAL AERONAUTICS AND SPACE ADMINISTRATION
WASHINGTON March 1960

[redacted]

NATIONAL AERONAUTICS AND SPACE ADMINISTRATION

TECHNICAL MEMORANDUM X-152

# INVESTIGATION OF A 4.0-INCH-MEAN-DIAMETER FOUR-STAGE REENTRY TURBINE FOR AUXILIARY POWER DRIVES*

By Robert Y. Wong, David L. Darmstadt, and Daniel E. Monroe

12795


## SUMMARY

A four-stage 4.0-inch-mean-diameter reentry turbine for auxiliary power applications was designed and investigated experimentally to study the problems associated with designing a reentry turbine for applications requiring high specific work output and very low weight flows.

The results of the experimental investigation indicated that at design equivalent speed and design pressure ratio (55.66) the equivalent specific work output in air was 35.95 Btu per pound at a total-to-static efficiency of 0.432. An analysis of the subject turbine indicated that partial admission and mass-flow deficits due to rotor pumping and seal leakage have an important effect on the overall efficiency of this turbine. In this analysis a theoretical efficiency of 0.519 was computed. The difference between the experimental and analytical efficiency may be attributed to the effects of mismatch in stator areas between the third and fourth stages, mixing losses due to the effects of the relatively large trailing-edge thicknesses used, and seal-leakage flows.


Author

## INTRODUCTION

In order to minimize the gross weight of an auxiliary drive system, it is necessary that the turbine extract maximum work from each pound of fuel expended. Therefore, the turbine must be designed for maximum inlet total enthalpy and high overall pressure ratio, and reasonable overall turbine efficiency must be attainable. To achieve a reasonable overall turbine efficiency under these conditions and be consistent with stress-limited rotor blade speeds, multistaging of the turbine must be employed. If a conventional full-admission design were used, the low weight-flow requirements of auxiliary power turbines would result in initial stage blade heights that would be too small to be practical. Partial admission can be used to solve the problem of short blade height. The multiple-reentry turbine also appears to have considerable potential over full-admission multistage designs for auxiliary power applications.

*Title, Unclassified.

[redacted]

This advantage stems from the fact that the multistaging is accomplished by passing the flow through a single rotor several times. Changes in density from stage to stage are compensated for with changes in the arc of admission. This makes possible practical blade heights in the initial stages. In the case where the rotor stress limits the turbine-inlet temperature, the cooling effect on the rotor by the later stages makes operation possible at higher inlet temperatures than with a conventional design. The multiple-reentry turbine also has the advantage of simplicity and possible reduction of weight of the rotating components.

The performance of a three-stage reentry turbine is given in reference 1. This reference turbine was designed for a fairly low pressure ratio (10:1) and a moderately high weight flow as compared with design requirements for turbines with auxiliary-power-unit applications. The ducting used to collect and redirect the flow at high velocity between stages required a complicated fabrication procedure to minimize pressure loss.

In order to investigate the problems associated with the use of multiple-reentry turbines for low-weight-flow, high-specific-work-output applications, a four-stage reentry turbine was designed and experimentally investigated. The turbine was designed to eliminate the need for complicated ducting by diffusing the flow at the rotor exit to a low velocity before entering the ducting and then accelerating the flow in a conventional stator blade row. Further, the design of the subject turbine differs from the reference turbine in that the sum of the arcs of admission of the four stages totals approximately 262° while the reference turbine used 360° as the total of the arcs of admission. An analysis of the geometry of the subject turbine was made to indicate the problem areas, and their analysis - in addition to the results of the investigation - is presented herein.

## SYMBOLS

$g$ gravitational constant, 32.17 ft/sec$^2$

$\Delta H$ equivalent specific work output in air, Btu/lb,

$$\frac{\Delta h}{\theta_{cr}}\left(\frac{V^*_{cr,air}}{V^*_{cr,working\ fluid}}\right)^2$$

$\Delta h$ specific work output, Btu/lb

$J$ mechanical equivalent of heat, 778 ft-lb/Btu

$N$ equivalent speed in air, rpm

[redacted]

| | |
|---|---|
| $p$ | absolute pressure, lb/sq ft |
| $U$ | blade velocity, ft/sec |
| $V$ | absolute gas velocity, ft/sec |
| $W$ | relative gas velocity, ft/sec |
| $w$ | weight-flow rate, lb/sec |
| $\delta$ | ratio of turbine-inlet total pressure to NASA standard sea-level pressure, $p_0'/p^*$ |
| $\eta_{fa}$ | adiabatic efficiency for full-admission operation |
| $\eta_{pa}$ | adiabatic efficiency for partial-admission operation |
| $\eta_s$ | adiabatic efficiency, ratio of blade power to ideal blade power based on total-to-static pressure ratio |
| $\eta_w$ | adiabatic efficiency including the effects of partial admission and mass-flow deficits due to seal leakage and rotor pumping |
| $\theta_{cr}$ | squared ratio of critical velocity at turbine inlet to critical velocity at NASA standard sea-level temperature $(V_{cr,0}/V_{cr}^*)^2$ |
| $\lambda$ | speed-work parameter, $\frac{U_m^2}{gJ\,\Delta h}$ |
| $\nu$ | blade-jet speed ratio, $\frac{U_m}{\sqrt{2gJ\,\Delta h_{id}}}$ |
| $\sigma$ | solidity, ratio of chord length to blade spacing |
| $\tau$ | torque, in.-lb |

Subscripts:

| | |
|---|---|
| cr | conditions at Mach number of unity |
| id | ideal |
| m | mean radius |
| x | axial direction |
| 0 | station at turbine inlet |
| 1 | station just upstream of trailing edge of first-stage stator |

3 station at inlet to second stage

4 station just upstream of trailing edge at second-stage stator

6 station at inlet to third stage

7 station just upstream of trailing edge for third-stage stator

9 station at inlet to fourth stage

10 station just upstream of trailing edge of fourth-stage stator

12 at discharge of turbine

Superscripts:

* NASA standard sea-level conditions

' absolute total state

## TURBINE DESIGN

The following characteristics (based on air as the working fluid) were selected as being typical of those for an auxiliary-power-drive turbine:

Equivalent air weight flow, $w\sqrt{\theta_{cr}}/\delta$, lb/sec . . . . . . . . . . . 0.00429
Equivalent mean wheel speed, $U_m/\sqrt{\theta_{cr}}$, ft/sec . . . . . . . . . . . . 400
Mean wheel diameter, in. . . . . . . . . . . . . . . . . . . . . . . . . . 4.0
Blade height, in. . . . . . . . . . . . . . . . . . . . . . . . . . . . . 0.125

### Stage Design Characteristics

Stage speed-work parameters $\lambda$ of 0.25, 0.50, 0.50, and 0.50 were selected for the first to fourth stages, respectively. This particular work split was determined from consideration of minimizing the first-stage mass-flow deficit due to rotor pumping (see ANALYSIS OF RESULTS). From reference 2 and the selected stage speed-work parameters, stage efficiencies for full-admission operation were obtained and then arbitrarily reduced to account for anticipated Reynolds number effects. Stage efficiencies (based on total-to-static pressure ratio) of 0.60, 0.70, 0.70, and 0.70 were therefore used in the design for stages 1 to 4, respectively. These efficiencies, together with the selected speed-work parameters, result in stage total-to-static pressure ratios of 4.332, 2.045, 2.305, and 2.726 for stages 1 to 4, respectively, with an overall turbine total-to-static pressure ratio of 55.66 and overall blade-jet speed ratio $\nu$

of 0.194. An overall design efficiency is not discussed here because of anticipated losses that are peculiar to reentry turbines. These losses will reduce the overall efficiency from that used in the design, even though design velocity diagrams for each stage may be established.

In addition to the characteristics just mentioned, the following assumptions were also made in order to construct the stator- and rotor-inlet velocity diagrams:

(1) The axial clearance between the rotor leading edge and stator trailing edge is zero. (Thus, the velocity just upstream of the stator trailing edge is used to calculate the rotor-inlet diagrams.)

(2) The total-to-static pressure ratio of each stage is taken across the stator.

(3) The velocity head at the exit of each stage is completely lost in diffusion.

(4) The rotor-inlet and -outlet angle is specified equal to 35°. The inlet velocity diagrams for the stator and rotor, constructed at the mean radius as described for two-dimensional flow, are presented in figure 1. Figure 1 shows that the first-stage stator is designed to operate with a supersonic exit velocity ($(V/V_{cr})_1 = 1.433$), while for stages 2 to 4 the stator-exit absolute velocity ratios are 1.054, 1.129, and 1.222, respectively. The rotor-inlet absolute flow angles for stages 1 to 4 are 24.75°, 21.25°, 21.16°, 21.50°, respectively. The rotor-inlet relative velocity for the first stage is supersonic ($(W/W_{cr})_1 = 1.178$), while the relative velocity ratios for the second to fourth stages are 0.710, 0.758, and 0.825, respectively.

## Blade Design

The first-stage stator was designed to give a smoothly converging channel to the throat. No analysis of the channel for surface velocity distribution was made because of the relatively large acceleration of the flow. At the throat a 2-percent area allowance was made to account for boundary-layer growth. From the throat, supersonic expansion to a critical velocity ratio $(V/V_{cr})_1$ of 1.433 was required. A minimum-length supersonic nozzle design was obtained by the method described in reference 3. An area allowance of approximately 5 percent was made between the throat and the nozzle exit to allow for additional boundary-layer growth. This was accomplished by designing the nozzle for an ideal supersonic velocity that corresponded to a 5-percent larger exit area. Table I gives the dimensions of the first-stage stator. Presented in figure 2 is the mean-radius channel profile for the first-stage stator.

The stator blades for the remaining stages were obtained by first laying out a smoothly converging channel with a blade spacing slightly larger than that required for the second stage. A trailing-edge thickness of 0.010 inch with sharp corners was used. When the spacing was reduced, a converging-diverging nozzle was obtained. Reducing the spacing coupled with slight changes in blade orientation resulted in the desired stator blade channel for each of the remaining stages. A 2-percent area allowance was also made for boundary-layer growth. The arc of admission required for each stage was computed on the assumption that the velocity head at the exit of each stage is completely lost. Thus, the static pressure at the exit of one stage was assumed equal to the total pressure at the inlet to the succeeding stage. Table I presents the blade orientation and spacing, arc of admission, number of channels, and throat dimensions for the stators. Figure 2 presents the stator blade profiles forming the mean-radius flow passages for the second to fourth stages. The sharp corners used on the trailing edge of the stator and on the leading and trailing edges of the rotor can be noted in the figure of table I.

The rotor blade profiles were laid out for the mean radius with zero stagger angle and with straight-line suction surfaces from the leading and trailing edges to the channel inlet and outlet, respectively. These straight lines were oriented at $35^{\circ}$ with the plane of rotation. A circular arc tangent to both straight lines at the channel entrance and exit was used to complete the suction surface. The pressure surface was obtained by using a circular arc tangent to these same flow angles at the leading and trailing edges. Sharp corners and a thickness of 0.005 inch were used on both the leading and trailing edges. In order to minimize surface velocity peaks, a relatively high solidity $\sigma$ of 2.5, which resulted in 125 blades, was used. The rotor blade profiles forming the mean-radius channels are given in figure 2. The rotor design specifications are given in table I.

## Return-Duct Design

The return ducts were designed such that at the exit of the rotor the flow is diffused to low velocity before being carried around to the stator inlet where it is reaccelerated. This diffusion was accomplished by varying the hub and tip radii linearly and in equal amounts so that the diffuser height at the exit was 1 inch. Since the inlet height was 0.125 inch, this gave an area ratio of 8. A projection of the return duct in the radial axial plane (section B-B) showing the diffuser (II) is given in figure 2. From the diffuser, the flow is turned $180^{\circ}$ and further diffused by an area change of approximately 2 to 1 (III). From the turn, the flow is ducted (IV) to another $180^{\circ}$ turn (V) where it is accelerated by an area reduction of 2 to 1. From the turn (V), the flow is accelerated (I) to the stator-entrance critical velocity ratio of approximately 0.2.

[redacted]





As discussed in reference 1, the placement of the collector is important in order to minimize loss of working fluids between stages, and its exact location requires a detailed knowledge of the flow path through the rotor. In lieu of a detailed study, the placement of the collector was based on the following simplifying assumptions. It was assumed that the two extremes of circumferential position for the jet to leave the plane of the rotor exit were: (1) that corresponding to the jet from the stator passing through the rotor undisturbed by rotor passages or diffusion, and (2) that corresponding to the jet leaving the exit plane of the rotor if the flow passed through the rotor undiffused and in an axial path. These assumptions established the extreme end points of the flow path at the rotor exit. The center of the collector was located midway between these extremes. The arc subtended by the collector was made $6^{\circ}$ larger than the arc of the stator exit for that stage. The width of the collector was enlarged to minimize loss of working fluids between stages and to account for spread of the jet due to mixing effects.

A cutaway sketch of the 4-inch-mean-diameter four-stage reentry turbine is presented in figure 3.

## APPARATUS, INSTRUMENTATION, AND PROCEDURE

The apparatus used in this investigation consisted of the subject turbine configuration, and suitable piping and controls to provide a uniform inlet flow to the turbine and exhaust into the laboratory altitude exhaust system. The rotor was coupled through a strain-gage torquemeter, a slip-ring assembly, and a speed-reducing gear box to a hydraulic-pump dynamometer. A diagrammatic sketch of the test rig is presented in figure 4.

High-pressure gaseous nitrogen was chosen as a working fluid for this turbine because of its availability at high pressures and low dewpoint.

Since the stator was designed to operate at choked conditions, the equivalent choking weight flow was determined with a calibrated rotameter prior to taking performance data. The equivalent choking weight flow was assumed constant for computing turbine performance. Turbine speed was measured with a magnetic pickup and a ten-tooth sprocket gear mounted on the rotor shaft in conjunction with an electronic tachometer.

The torque output of the shaft was measured with a strain-gage torquemeter similar to that used in reference 4. Turbine-inlet total pressure was measured with a static tap at a point of low Mach number where total-to-static pressure ratio can be assumed to be close to 1.0.

Interstage and outlet pressure measurements were made with static taps in the return ducts and outlet duct, respectively. Temperatures

[redacted]

were measured at the turbine inlet and outlet with thermocouples placed in the plenum upstream of the first-stage stator and in the exhaust duct.

The experimental data were obtained by operating the turbine over a range of pressure ratios and speeds. Inlet conditions were maintained at nominal values of 200 pounds per square inch absolute and 120° F. The outlet pressure was varied to give a total-to-static pressure ratio range of from 20 to 100 nominally. Turbine speed was varied from 40 to 100 percent of design speed (approx. 24,000 rpm) in increments of 20 percent.

E-450

Rotor blade power (used to rate turbine) was obtained by adding bearing loss to measured shaft power. The bearing loss was obtained by removing the rotor, motoring the shaft at various speeds, and measuring bearing torque with a strain-gage torquemeter. The bearing power was 5.9 percent of the measured shaft power at design speed and pressure ratio.

Turbine efficiency was computed as the ratio of rotor blade power to ideal rotor blade power. The ideal rotor blade power with nitrogen as a working fluid was obtained from a temperature-entropy diagram, measured inlet total pressure and temperature, and outlet static pressure. The temperature-entropy diagram was obtained from real gas properties presented in reference 5.

Equivalent specific work in air $\Delta H$ was computed by multiplying the equivalent specific work in nitrogen by the squared ratio of the critical velocities in each fluid.

## RESULTS AND DISCUSSION

The experimentally obtained performance of the four-stage reentry turbine is shown in figure 5. In this figure, equivalent specific work output $\Delta H$ with air as a working fluid is plotted against total-to-static pressure ratio $p_0'/p_{12}$. Lines of constant efficiency $\eta_s$ are also shown. At design equivalent speed and design pressure ratio, the equivalent specific work output was 35.95 Btu per pound and the efficiency was 0.432. The observed choking equivalent air weight flow was 0.0044 pound per second, which was 3.5 percent greater than the design value of 0.00429. The higher observed weight flow was found to have resulted from approximately a 3-percent larger throat area than was designed.

In figure 6 is presented the static-pressure distribution through the turbine at design speed and design pressure ratio. These static pressures were measured in the various return ducts (IV of fig. 2) and are given as ratios to the inlet total pressure. For comparison, the design static-pressure variation, together with the stage pressure ratios, is shown. In general, the experimentally obtained pressure distribution through the turbine was reasonably close to design distribution except for the third stage. This indicates that the fourth stage was choking before design pressure ratio could be achieved across the third stage. Further, design free-stream velocity diagrams were closely approximated.

The torque-speed characteristics at design pressure ratio for the subject turbine are presented in figure 7. It can be seen that the turbine zero speed torque is twice that at design speed. Further, the torque varies linearly with speed. These characteristics are comparable with conventional full-admission designs having similar stage-speed and specific-work requirements.

## ANALYSIS OF RESULTS

The results of the experimental investigation gave an overall efficiency of 0.432. This is noted to be considerably different from an overall efficiency obtainable from the stage efficiencies of 0.60, 0.70, 0.70, and 0.70 that were used in the design. Thus, the losses peculiar to reentry turbines appear to be significant; and, in order to determine their magnitude, an analysis was made.

The analysis consisted of first obtaining theoretical full-admission efficiencies for the geometry of the various stages operating at their respective design velocities and design Reynolds numbers. These theoretical efficiencies were then reduced for the effects of partial admission and mass-flow deficit due to rotor pumping and seal leakage. An overall efficiency was obtained and was compared with that obtained experimentally.

The theoretical full-admission efficiency for the various stages was obtained by the method of reference 6. This method uses blade-jet speed ratio, rotor and stator turning angle, aspect ratio, a tip clearance factor, and a characteristic Reynolds number to predict stage performance for a strictly impulse turbine. Full-admission stage efficiencies $\eta_{fa}$ of 0.5607, 0.6559, 0.6368, and 0.6066 were predicted for stages 1 to 4, respectively. These efficiencies are of the same order of magnitude as was predicted by the method of reference 4, which uses speed-work parameter and a Reynolds number based on blade height as the criteria. It should be noted that these efficiencies are somewhat lower than those used in the design. The predicted efficiencies are plotted in a bar graph in figure 8 for future reference. The overall efficiency including reheat is 0.683.

The effect of partial admission on stage performance was evaluated by the method presented in reference 7. These effects include mixing losses, scavenging losses, and a momentum loss due to filling of the inactive passages and emptying the active passages as they are brought into and out of the jet. The method also uses the ratio of the length of stator discharge arc to rotor blade spacing as a prime variable. This method is similar to that presented in reference 6 except that the momentum-loss term was increased. By use of equation (3) of reference 7, the stage efficiencies for partial-admission $\eta_{pa}$ operation (computed from full-admission efficiencies $\eta_{fa}$ obtained earlier) are 0.4270, 0.5798, 0.6002, and 0.5913 for stages 1 to 4, respectively. These efficiencies are plotted in figure 8. Comparison of these efficiencies with the calculated full-admission stage efficiency indicates that there is a 13.37-point drop in first-stage efficiency because of partial-admission effects. Further, there was a 7.61-point drop in efficiency predicted for the second stage. There were only minor decreases in efficiency predicted for the third and fourth stages because of the relatively large arc of admission as compared with the rotor blade spacing. A new overall efficiency including reheat was computed to be 0.609, which reflects a drop of 0.074 due to partial-admission effects.

An evaluation of the effect of mass-flow transfer within the turbine due to seal leakage and rotor blade-passage pumping was obtained as follows. Rotor blade-passage pumping weight flow was computed as the product of rotor volume flow and static density at the stator outlet of the stage. Thus, in order to minimize first-stage pumping, the stator-outlet static pressure was minimized by increasing the first-stage pressure ratio. Increasing the first-stage pressure ratio resulted in the work split described in "Stage Design Characteristics." Rotor-hub seal-leakage weight flow was computed on the basis of the following model. The inlet hub fairing and outlet hub fairing, which are separated by the rotor disk, form two plenum chambers that are subjected to the various static pressures of each stage. Turbine working fluids will leak into or out of these plenum chambers, depending on the static pressure of the stage. The assumption was made that the equilibrium pressure within each plenum is determined by a weight-flow balance between the flow coming into it from the first two stages and the flow going out of the plenum and into the last two stages. Further, it was assumed that the area of leakage of a given stage is proportional to the arc of the rotor exposed to the flow plus the arc of the divider between that stage and the succeeding stage. A flow coefficient of 0.35 was used to compute the seal-leakage weight flow. This coefficient was selected from figure 82 of reference 8. In this figure a range from approximately 0.2 to 0.35 is presented for a clearance of 0.0045 inch; the upper limit was selected because the particular seal design appears to have been less than optimum. A well-designed seal would have resulted in seal weight flow of about one-half of that for the design used herein.

The rotor-pumping and seal-leakage weight flows computed as just described are presented in table II as the percent of turbine-inlet weight flow. In this table the negative values indicate a removal of the flow from the stage, and positive values indicate that the flow direction

DECLASSIFIED

[redacted]



E-450

CP-2 back

is into the stage. It can be seen that the rotor-pumping weight flow varies from 35.2 to 3.7 percent of the turbine-inlet weight flow. Seal-leakage weight flow varies from 2.0 to 5.6 percent of turbine-inlet weight flow. The effect of rotor pumping and seal leakage on stage performance is obtained for the first two stages from the partial-admission efficiencies previously computed and from the following equation:

$$\eta_w = \eta_{pa}\left(\frac{\text{Stator weight flow - Seal flow at rotor entrance}}{\text{Turbine-inlet weight flow}}\right)$$

In the case of the third and fourth stages, the seal flow entering the stage upstream of the rotor was considered to do no work in that stage; therefore, only the stator weight flow was used in the following equation:

$$\eta_w = \eta_{fa}\left(\frac{\text{Stator weight flow}}{\text{Turbine-inlet weight flow}}\right)$$

The efficiencies computed for stages 1 to 4 are 0.4092, 0.3310, 0.4355, and 0.4990, respectively, and are plotted in figure 8. It is seen that weight-flow loss in the first stage resulted only in a minor change (1.78 points) in efficiency. For the second stage there was a reduction of 24.88 efficiency points because of seal-leakage and rotor-pumping weight flow. In the third and fourth stages 17.47 and 8.23 efficiency points were lost. The overall efficiency including reheat was reduced by 0.090 to 0.519 by the effects of mass-flow loss resulting from rotor pumping and seal leakage. Comparison of this efficiency with that obtained for full-admission operation (0.683) indicated that the losses peculiar to this type of reentry turbine are significant. Further, a comparison of the finally computed overall efficiency (0.519) with that obtained experimentally (0.432) indicated that there are still other significant losses which have not been considered. Some of these losses can be attributed to the mismatch between the stator throat area of the third and fourth stages. Another factor to be considered is the relatively thick rotor and stator trailing edges that produce thicker blade wakes and, in turn, increase the mixing losses. Further, the momentum losses associated with the seal-leakage flow into the third and fourth stages may also have been a factor.

## SUMMARY OF RESULTS

The results of the investigation of the 4.0-inch-mean-diameter four-stage reentry turbine can be summarized as follows.

At design equivalent speed and design pressure ratio, an equivalent work output in air of 35.95 Btu per pound was obtained at a total-to-static efficiency of 0.432. At this operating condition, design pressure

[redacted]

distribution through the stages was obtained with the exception of the third-stage exit.

An analysis of the subject turbine indicated that the losses peculiar to this type of reentry turbine can significantly reduce the overall efficiencies. Penalties in efficiencies for this unit, as a result of partial-admission effects and mass-flow deficits due to rotor pumping and seal leakage, were computed to be 0.074 and 0.090, respectively, with an overall efficiency of 0.519. Comparison of this overall efficiency with that computed for full-admission operation (0.683) indicates that these two losses associated with this reentry turbine are significant. The difference between the computed overall efficiency (0.519) and that obtained experimentally (0.432) may be attributed to the effects of mismatch between the stator throat areas of the third and fourth stages and large trailing-edge blockages, as well as momentum losses associated with the seal-leakage flow into the third and fourth stages.

E-450

Lewis Research Center
National Aeronautics and Space Administration
Cleveland, Ohio, November 23, 1959

## REFERENCES

1. Evans, David G.: Design and Experimental Investigation of a Three-Stage Multiple-Reentry Turbine. NASA MEMO 1-16-59E, 1959.

2. Stewart, Warner L.: Analytical Investigation of Multistage-Turbine Efficiency Characteristics in Terms of Work and Speed Requirements. NACA RM E57K22b, 1958.

3. Edelman, Gilbert M.: The Design, Development, and Testing of Two-Dimensional Sharp-Cornered Supersonic Nozzles. Rep. 22, M.I.T., May 1, 1948. (Bur. Ord. Contract NOrd 9661.)

4. Wong, Robert Y., and Monroe, Daniel E.: Investigation of 4.5-Inch-Mean-Diameter Two-Stage Axial-Flow Turbine Suitable for Auxiliary Power Drives. NASA MEMO 4-6-59E, 1959.

5. Hilsenrath, J., et al.: Tables of Thermal Properties of Gases. Cir. 564, NBS, Nov. 1, 1955.

6. Stenning, Alan H.: Design of Turbines for High-Energy-Fuel Low-Power-Output Applications. Rep. 79, Dynamic Analysis and Control Lab., M.I.T., Sept. 30, 1953.

[redacted]



7. Mann, Robert W.: Fuels and Drive Movers for Rotating Auxiliary Power Units. Rep. 121, M.I.T., 1957.

8. Stodola, A.: Steam and Gas Turbines. Vol. I. McGraw-Hill Book Co., Inc., 1927. (Reprinted, Peter Smith (N.Y.), 1945.)

[redacted]

[redacted]

E-450

TABLE I. - BLADE DESIGN INFORMATION

First-stage stator

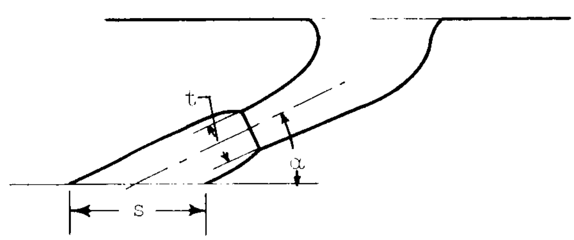


Second to fourth-stage stator

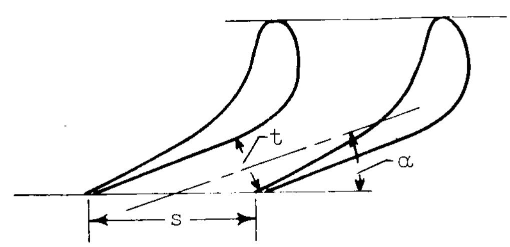


| Specifications | Stage | | | |
|---|---|---|---|---|
| | 1 | 2 | 3 | 4 |
| α | 24°45' | 21°15' | 21°10' | 21°30' |
| t, in. | 0.102 | 0.130 | 0.107 | 0.085 |
| s, in. | 0.314 | 0.384 | 0.336 | 0.280 |
| Number of passages | 1 | 3 | 7 | 19 |
| Percent arc of admission | 2.5 | 9.2 | 18.7 | 42.3 |

Rotor blading

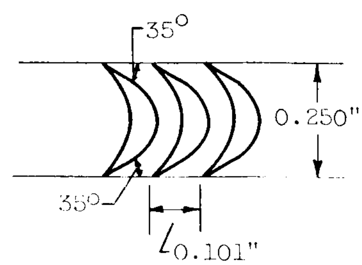


[redacted]

E-450

TABLE II. - COMPUTED LEAKAGE LOSSES WITHIN TURBINE

| Stage | Weight flow into stator | Seal flow at rotor entrance | Rotor flow | | Seal flow at rotor exit | Net flow into collector |
|---|---|---|---|---|---|---|
| | | | In | Out | | |
| 1 | 100.0 | -4.2 | 3.7 | -35.2 | -3.8 | 60.5 |
| 2 | 60.5 | -3.4 | 35.2 | -16.6 | -3.2 | 72.5 |
| 3 | 72.5 | 2.0 | 16.6 | -8.3 | 1.6 | 84.4 |
| 4 | 84.4 | 5.6 | 8.3 | -3.7 | 5.4 | 100.0 |

[redacted]

E-450

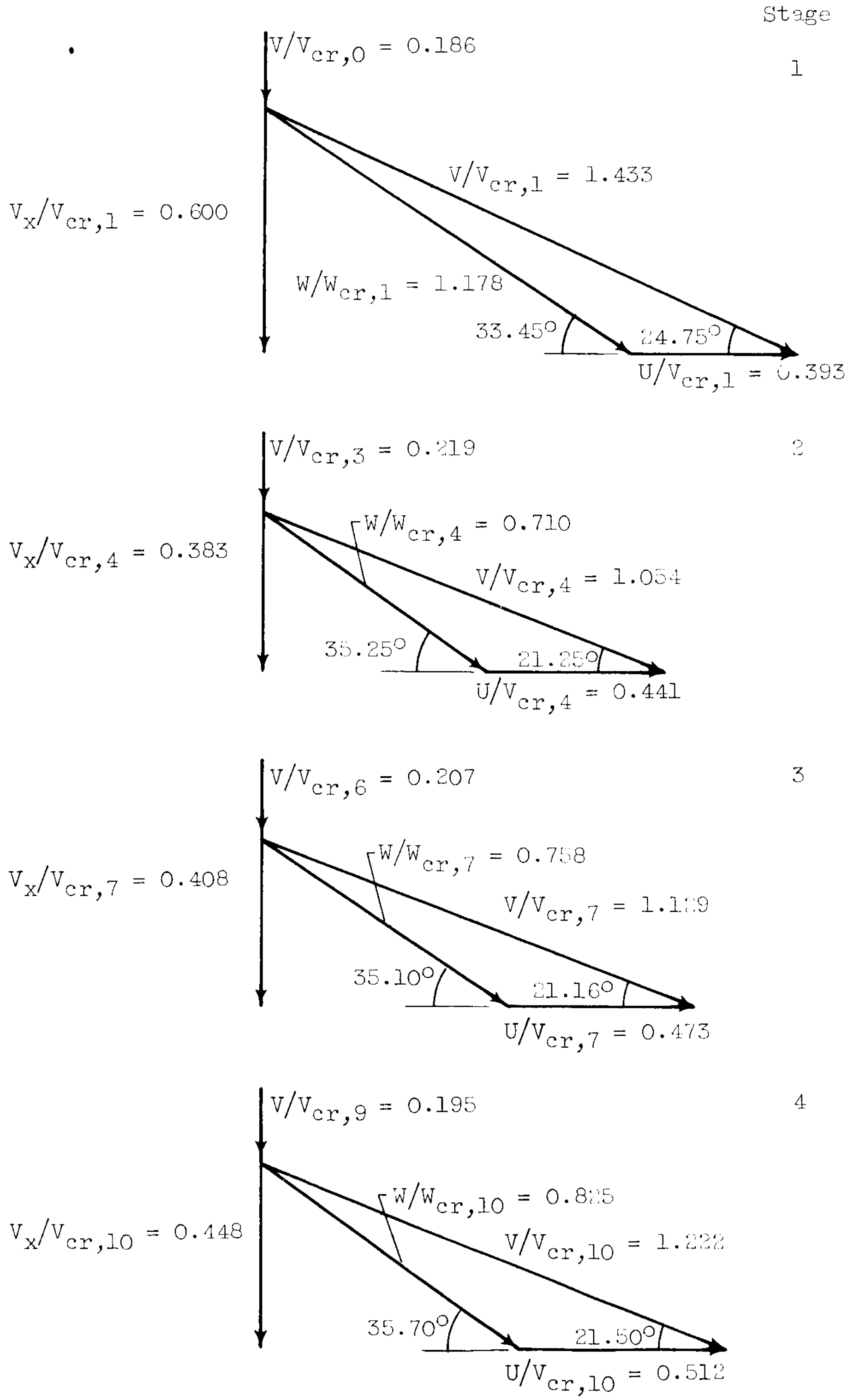


Figure 1. - Design velocity diagrams for 4-inch-mean-diameter four-stage reentry turbine.

[redacted]

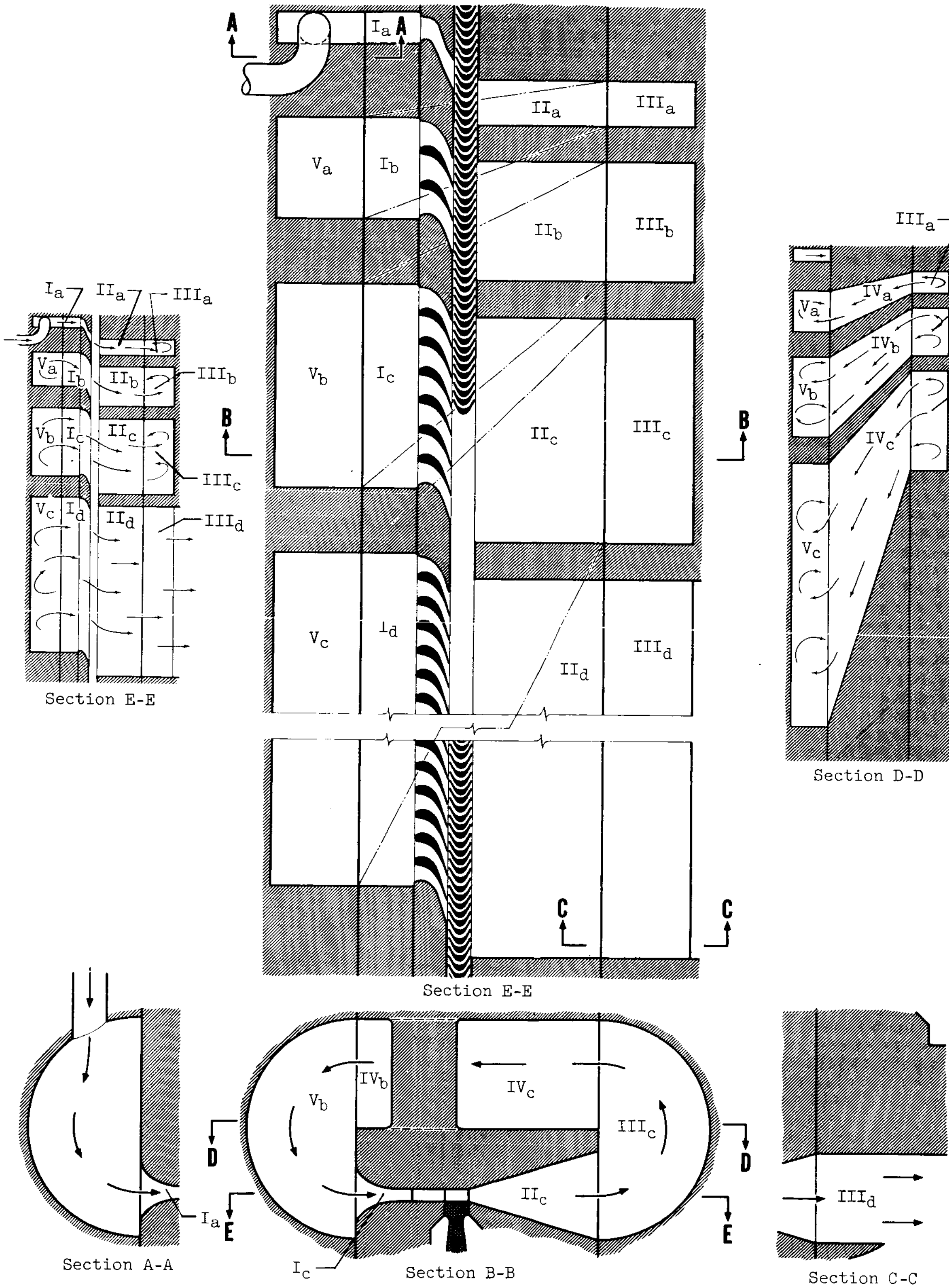


Figure 2. - Layout of turbine configuration.

CD-6726

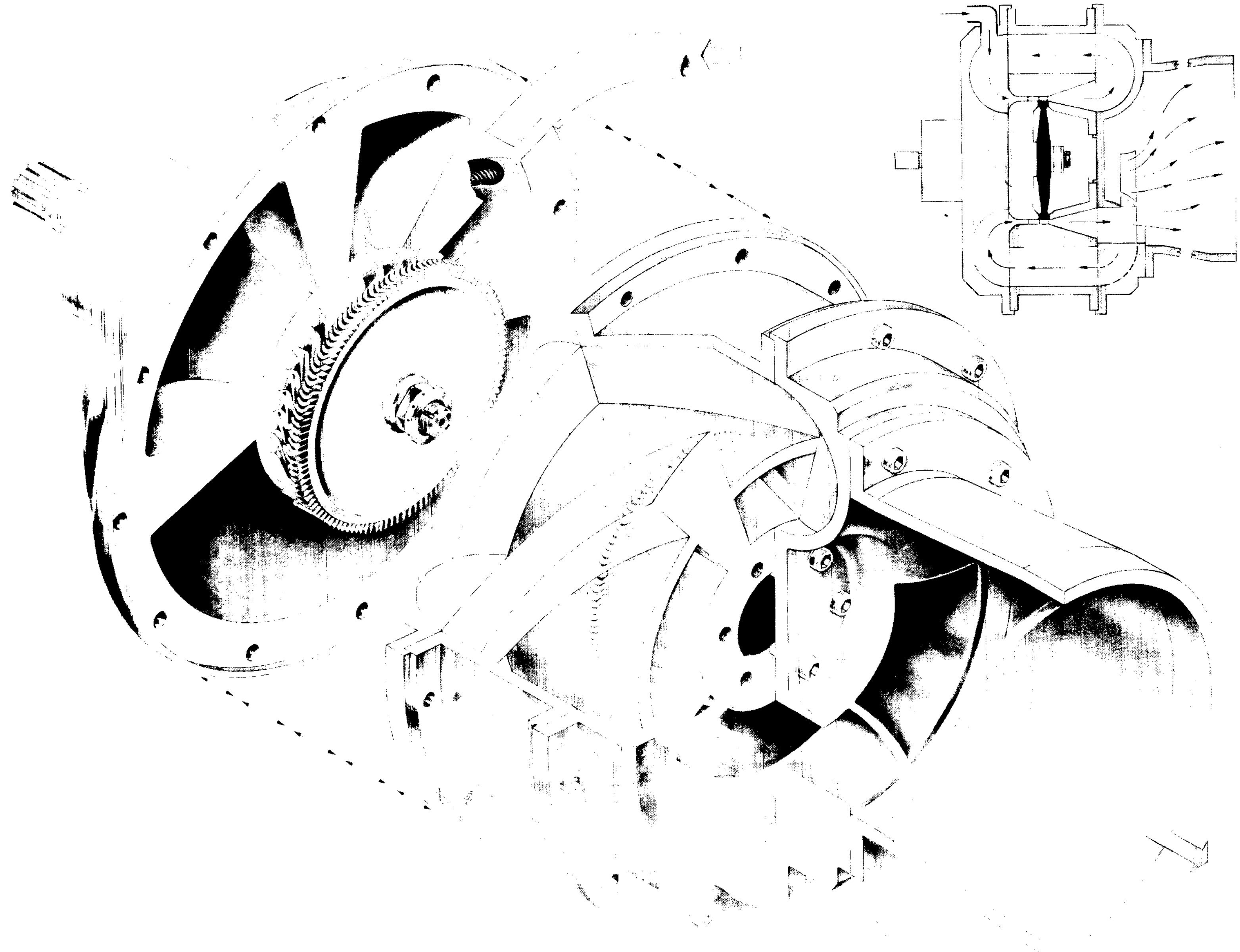

CD-6598

Figure 3. - Cutaway sketch of 4-inch-mean-diameter four-stage reentry turbine.

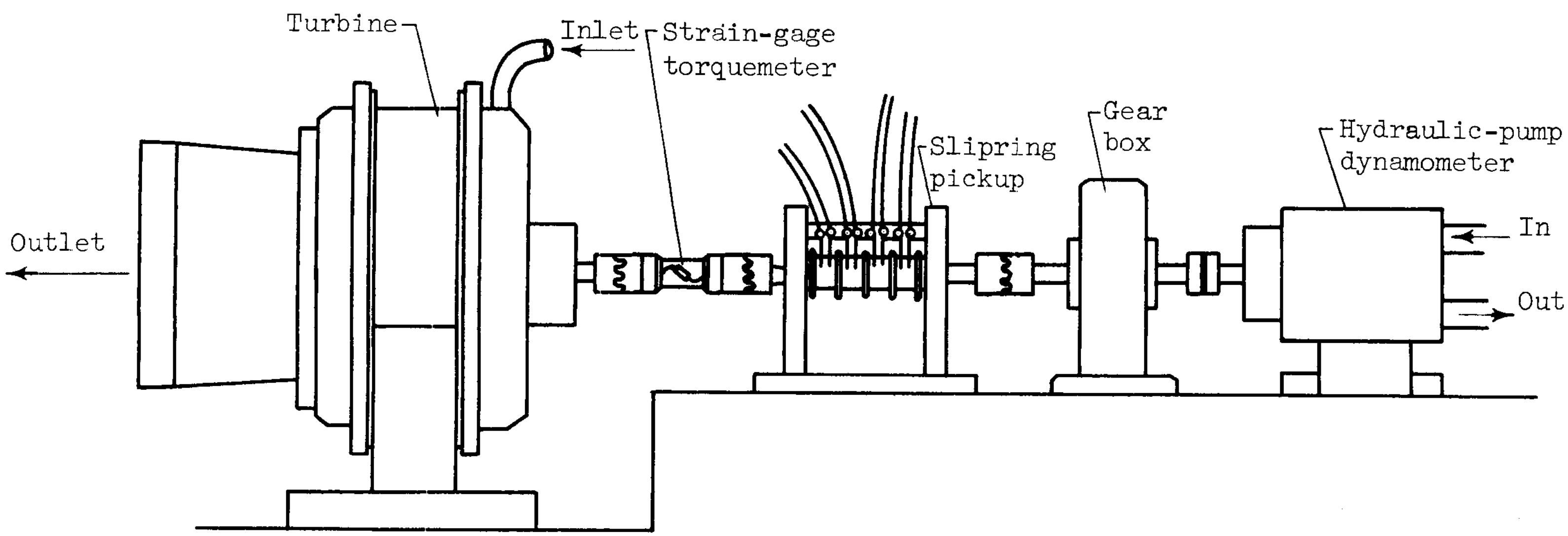


Figure 4. - Test apparatus.

[redacted]

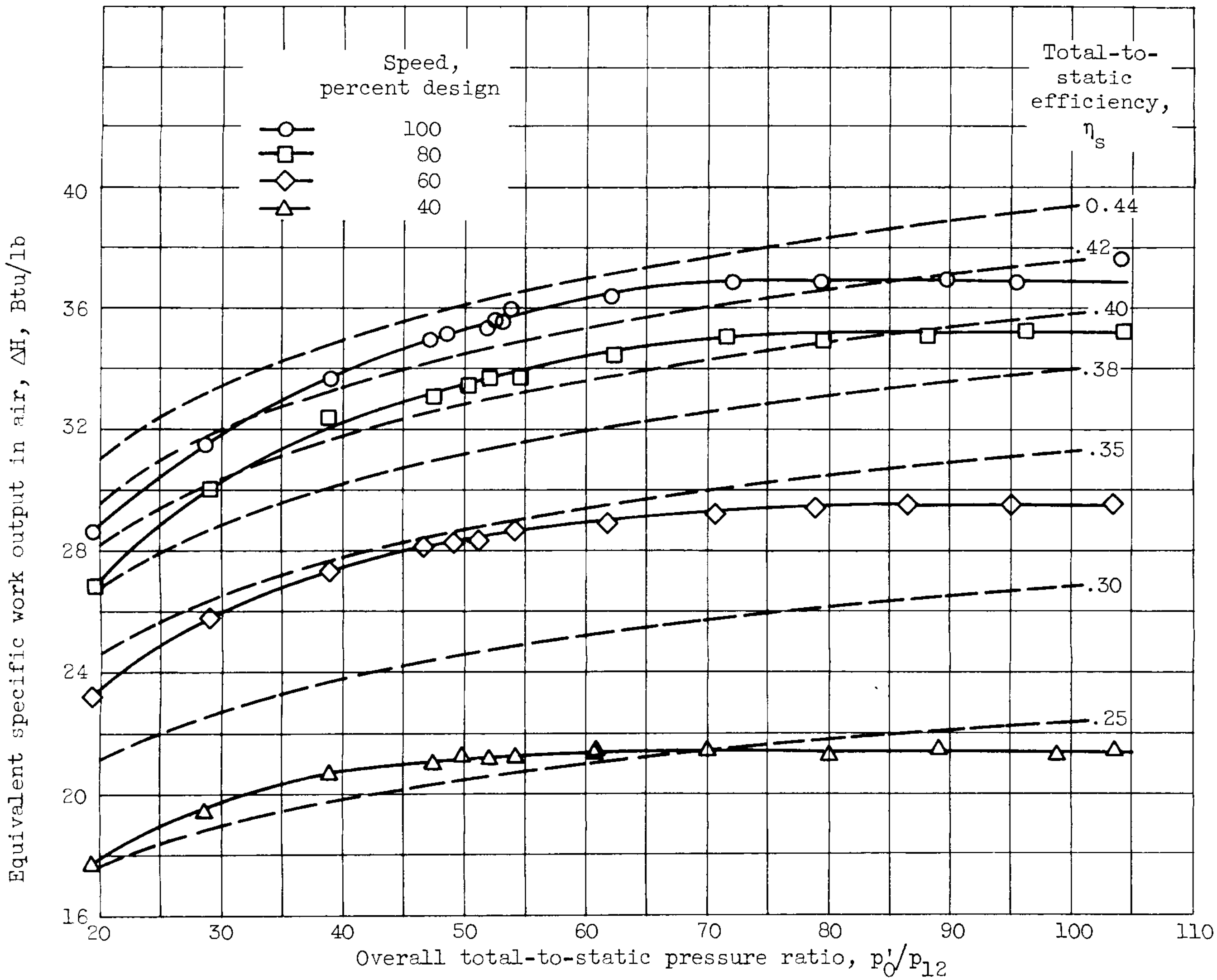


Figure 5. - Experimentally obtained performance of 4.0-inch-mean-diameter four-stage reentry turbine.

E-450

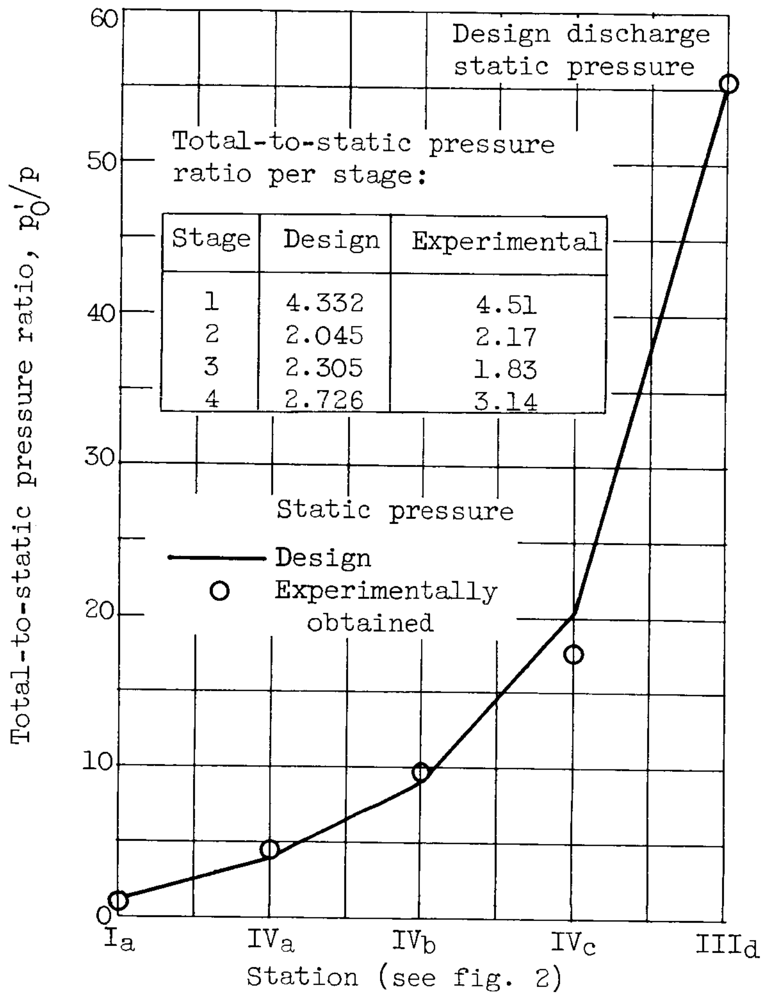


Figure 6. - Interstage static-pressure distribution.

[redacted]

[redacted]

E-450

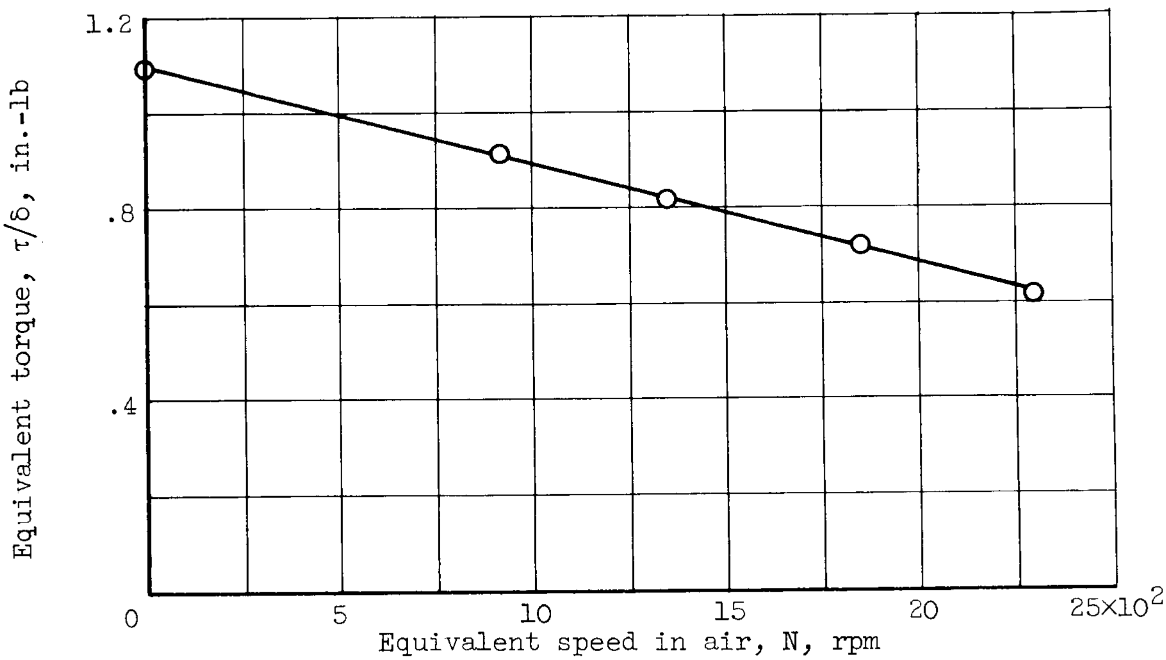


Figure 7. - Variation of torque with speed at approximately design pressure ratio.

[redacted]

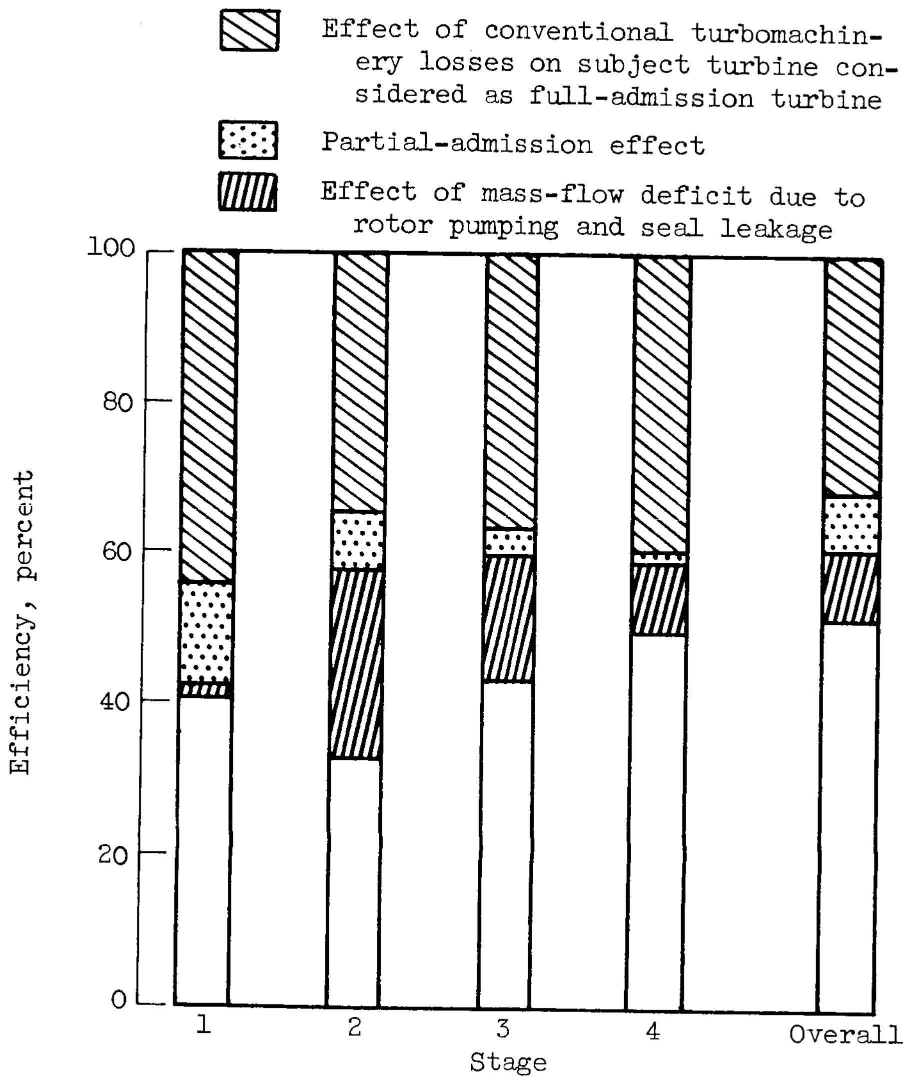


Figure 8. - Predicted efficiency based on overall total-to-static pressure ratio.